Applied Information Systems Research (AISR) Program

Final Report for NNG05EB61I
Fault-Tolerant Parallel-Processing Astronomical Image-Analysis Tools

PI: Kenneth J. Mighell (National Optical Astronomy Observatory)

Summary

With his first two-year AISR grant S-13811-G, the Principal Investigator (PI) demonstrated that precise and accurate stellar photometry and astrometry is possible and practical with ugly space-based PSFs which have high spatial frequencies rarely seen in ground-based astronomy due to the blurring of the Earth's atmosphere.

The AISR-funded MATPHOT[1] stellar photometry code uses discrete (sampled) Point Spread Functions consisting of a numerical table represented by a matrix in the form of a FITS[2] image. Discrete PSFs are shifted within an observational model using a 21-pixel-wide damped sinc function, and position partial derivatives are computed using a five-point numerical differentiation formula. Precise and accurate stellar photometry and astrometry are achieved with undersampled observations by using supersampled discrete PSFs that are sampled 2, 3, or more times more finely than the observational data. Although these numerical techniques are not mathematically perfect, they are sufficiently accurate for precision stellar photometry and astrometry due to photon noise which is present in all astronomical imaging observations [1]. The current C-language implementation [3] of the MATPHOT algorithm is based on a robust implementation[4, 5] of the Levenberg[6]-Marquardt[7] method of nonlinear least-squares minimization. Detailed analysis of simulated space-based CCD stellar observations demonstrate that millimag photometric precision and millipixel relative astrometry is achievable with complicated discrete PSFs[1].

With the transition funding provided by the one-year AISR grant NNG05EB61I, the PI was able to extend his MATPHOT algorithm and software to the point where it is now has the potential of enhancing the science return of *existing* NASA undersampled near-infrared imagers like the InSb detectors (3.6 and 4.5 microns) of the *Spitzer Space Telescope*'s Infrared Array Camera (IRAC) instrument.

This grant has yielded two published papers[8, 9] from two invited talks, *Innovative image analysis software as a technology driver for advances in space telescope design* and *Analysis of K-band imaging of the wide binary system σ CrB with the Lick Observatory NGS AO system*, which were given by the PI at the SPIE International Symposium Astronomical Telescopes and Instrumentation 2006 which was held in Orlando, Florida on May 24-31, 2006. Preliminary results were presented in a poster [10], *Mitigating the Impact of Large Intrapixel Quantum Efficiency Variations on Precision Stellar Photometry and Astrometry*, at the 207th meeting of the American Astronomical Society on January 9, 2006 in Washington, D.C.

AISR Grant NNG05EB61I Results

The following is an extract from the Infrared Array Camera (IRAC) Data Handbook[11]:

> The flux density of a point source measured from IRAC images depends on the exact location where the peak of the Point Response Function (PRF) falls on a pixel. This effect is due to the variations in the quantum efficiency of a pixel, and combined with the undersampling of the PRF, it is most severe in channel 1. The correction can be as much as 4% peak to peak. The effect is graphically shown in Figure 5.1 where the normalized measured flux density (y-axis) is plotted against the distance of the source centroid from the center of a pixel. The correction for channel 1 can be calculated from
>
> $$Correction = 1 + 0.0535 \times \left[\frac{1}{\sqrt{2\pi}} - p \right] \tag{5.14}$$
>
> where p is the pixel phase ($p = \sqrt{(x - x_0)^2 + (y - y_0)^2}$), where x, y, is the centroid of the point source and x_0 and y_0 are the integer pixel numbers containing the source centroid. The correction was derived from photometry of a sample of stars, each star observed at many positions on the array. The "ratio" on the vertical axis in Figure 5.1 is the ratio of the measured flux density to the mean value for the star. To correct the flux of a point source, calculate the correction from Equation 5.14 and divide the source flux by that correction. Thus, the flux of sources well-centered in a pixel will be reduced by 2.1%. Pixel phase corrections for other channels, if necessary, and after they have been more accurately determined than currently, will be given in future Data Handbook versions.

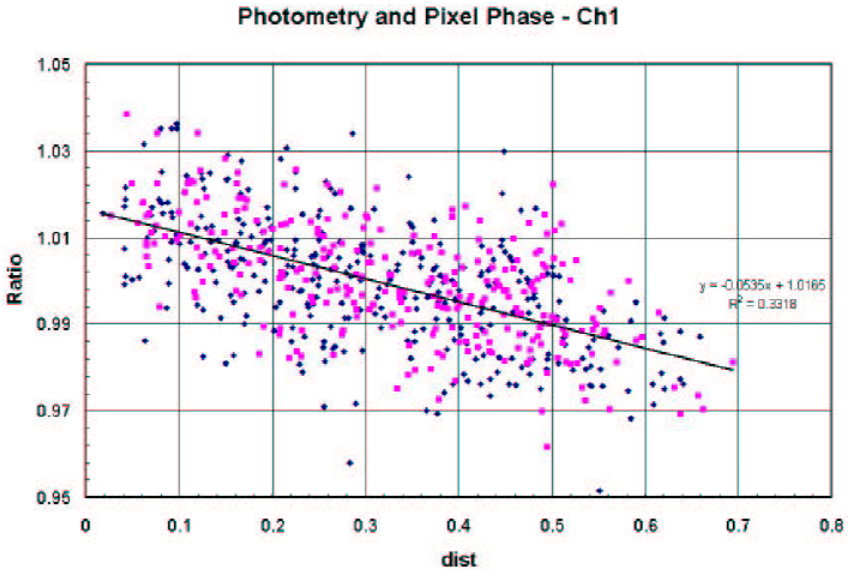

Figure 5.1: Dependence of point source photometry on the distance of the centroid of a point source from the nearest pixel center in channel 1. The ratio on the vertical axis is the measured flux density to the mean value for the star, and the quantity on the horizontal axis is the fractional distance of the centroid from the nearest pixel center.

Following discussions with *Spitzer Space Telescope*'s Infrared Array Camera (IRAC) team members at the 207th meeting of the AAS in January 2006 in Washington, D.C., the PI started working with various IRAC team members with the goal of determining if it might be possible to improve stellar photometry from IRAC's Channel 1 (3.6μ) by creating an experimental version of the existing MATPHOT code with an effective intrapixel quantum efficiency map for IRAC Ch1 hard-wired into the code.

Bill Hoffmann, an IRAC team member at the University of Arizona, has recently made the first estimate of the intrapixel QE variation across a single IRAC Channel 1 pixel:

$$\text{intrapix} = \begin{pmatrix} 0.813 & 0.875 & 0.875 & 0.875 & 0.813 \\ 0.875 & 1.000 & 1.000 & 1.000 & 0.875 \\ 0.875 & 1.000 & 1.000 & 1.000 & 0.875 \\ 0.875 & 1.000 & 1.000 & 1.000 & 0.875 \\ 0.813 & 0.875 & 0.875 & 0.875 & 0.813 \end{pmatrix}.$$

The mean conversion efficiency of this 5×5 convolution matrix is 91.01%. This is actually the *relative* intrapixel QE map since the central subpixels of this map were arbitrarily set to one; while the quantum efficiency of IRAC Channel 1 is high, the actual *absolute* values for the central subpixels are likely to be less than one. Full details about the derivation of this intrapixel quantum efficiency map may be found in Hoffmann's report *Intra-pixel Variation Effect on Aperture Photometry* [12].

Hoffmann[13] has computed theoretical 5×5 supersampled versions of the IRAC Ch1 PSF across the camera's field-of-view. Fig. 1 shows the model PSF which was computed for the central region of the IRAC Ch1. The left side of Fig. 1 shows a linear stretch of the PSF and the right side shows a log stretch. Although the PSF appears to be reasonable in the linear stretch, which emphasizes the bright central core, the log stretch shows the numerous weak higher-spatial-frequency features of this very complicated PSF. IRAC Ch1 PSFs are significantly undersampled by the IRAC Ch1 camera [14]; the mean effective background area[1] (a.k.a. the equivalent noise area[15]) is 7.0 pixels[16] as compared to the canonical value of 4π ($\sim$12.6 pixels) for a critically-sampled Gaussian PSF.

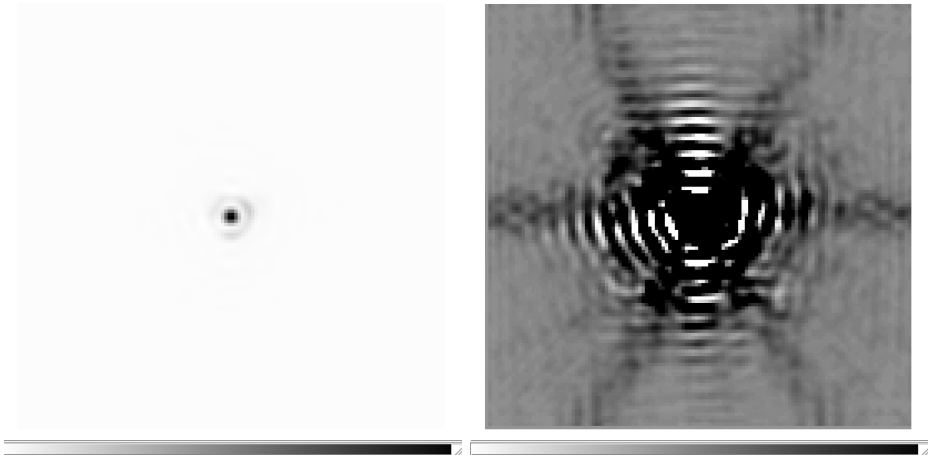

Figure 1: A theoretical 5×5 supersampled version of the IRAC Ch1 PSF.

Engineering decisions can significantly affect the science return of an instrument. The significant flux loss of IRAC Channel 1 is due to the combination of the non-negligible QE variation within a single pixel *and* the significant undersampling of the PSF by large (1.2 arcsec) pixels. The significant loss of flux in IRAC Ch1 could have been mitigated by simply oversampling the PSF. This capability was part of the initially proposed IRAC design which included both diffraction-limited and wide-field modes. The diffraction-limited mode was lost when the camera was simplified to include only the wide-field mode.

Image analysis software, which properly models the image formation process within the detector, has the *potential* of recovering the stellar flux lost by IRAC Ch1. Use of such software could thus enhance the science return from stellar (point source) observations which would appear, at first glance, to be limited to no better than 5% accuracy.

If an IRAC Ch1 observer follows the advice of the Infrared Array Camera Data Handbook [11] and uses the suggested correction formula (given above) to compensate for the lost stellar flux, then there will remain a variation of about 2% which is due to the fact that much of the *vertical variation seen in Fig. 5.1 of the IRAC Data Handbook is systematic* rather than random; the true flux correction function is a complicated two-dimensional distribution that is not circularly symmetric.

In a collaborative research effort with Bill Glaccum (Spitzer Science Center), Bill Hoffmann, and other IRAC team members, I have succeeded in creating a new experimental version of MATPHOT, called MPDY, which uses Hoffmann's intrapixel QE variation map [12] and the theoretical 5×5 supersampled PSF shown in Fig. 1 to create and analyze realistic IRAC Ch1 simulated observations.

Ten thousand IRAC Ch1 observations of a single star on a flat background were simulated and analyzed with MPDY. Each stellar observation was simulated using the theoretical 5×5 supersampled IRAC Ch1 PSF shown in Fig. 1; a star with 10^5 electrons was located near the center of 60×60 pixels on a flat background of 100 electrons (e^-). The efficiency of the photon to electron conversion process is calculated using the Hoffmann intrapixel QE map given above. Realistically noisy data was created by adding photon noise and a readout noise level of 3 e^- $pixel^{-1}$. Fig. 2 shows some of the results of the MPDY analysis of these simulations.

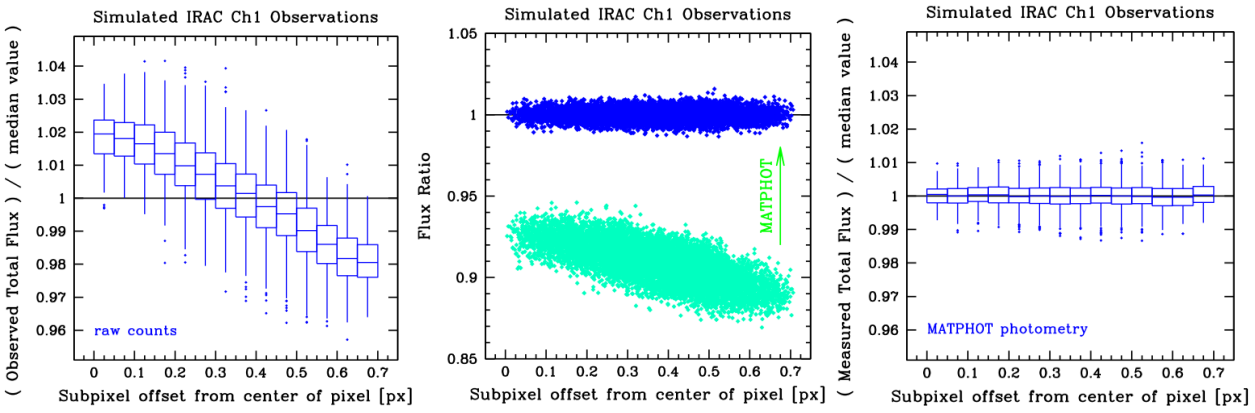

Figure 2: Results of the MPDY experiment with simulated IRAC Ch1 observations.

The horizontal axis of the left graph of Fig. 2 shows the subpixel offset (distance) the center of a star is from the middle of a pixel; stars centered near the middle of a pixel will have small offset values while stars located near the corner of a pixel will have offsets near 0.7 px. The vertical axis shows the *observed* (apparent) total flux divided by the *median observed* total flux value (90825.8 electrons, expected 100000) of all ten thousand stars. The median values of the box-and-whisker plots range from an excess flux of about 2% for stars centered near the center of a pixel to a flux deficit of about 2% for stars centered near the corner of a pixel. Note that this graph reproduces almost exactly the observed flux loss distribution seen in Fig. 5.1 of the IRAC Data Handbook [11].

The vertical axis of the central graph of Fig. 2 shows the absolute flux ratio of the total fluxes divided by the true flux of 10^5 electrons. The light grey (cyan) points show the *observed* absolute flux ratios and the black (blue) points show the *measured* absolute flux ratios as reported by MPDY. Note that while the average stellar observation suffered an absolute flux loss of ∼9%, stars centered near the middle of a pixel suffered, on average, an absolute flux loss of ∼7% as compared to an absolute flux loss of ∼11% for stars centered near a pixel corner. It is important to note that the vertical scatter seen in the observed flux ratios (absolute or relative) is not random but systematic; a simple radial correction function can only partially recover the lost flux. The measured absolute flux ratios are clustered around unity and are not a function of subpixel offset; the vertical scatter seen in the measured absolute flux ratios is random. By modeling the image formation process within the detector, MPDY was able fully recover all of the stellar flux lost due to the non-uniform IRAC Ch1 intrapixel quantum efficiency variations.

The vertical axis of the right graph of Fig. 2 shows the *measured* total flux (as reported by MPDY) divided by the *median measured* total flux value (99972.3 electrons, expected 100000) of all ten thousand stars. This graph shows that MPDY is able to recover the true stellar flux all the way down to the photon limit (photometric error of ∼3.9 millimag).

Non-uniform intrapixel QE maps can potentially cause significant systematic astrometric (position) errors for bright stars. Would we expect the IRAC Ch1 QE map to create systematic astrometric errors? Yes, indeed. If an intrapixel QE map is roughly circularly symmetric about the middle of a pixel (as is apparently the case for IRAC Ch1), then the centroid of an observed stellar image (i.e., the PRF) *which is centered in the middle of a pixel* will be approximately at the same position as the centroid of the PSF. However, if there is significant flux loss near the edges or corner of a pixel (as is apparently the case for IRAC Ch1), then the *centroid of a PRF which is centered near a pixel corner will most likely not be the same as the centroid of the PSF* — and the difference will be a systematic error rather than a random error.

The major component of the systematic astrometric error is the undersampling of the PSF by IRAC Ch1. The intrapixel QE variation in the detector just makes the matter a little worse. Naively doing centroiding on the recorded undersampled stellar image may lead to astrometry which has dubious value. However, photometric reduction codes that model the image formation process within the detector can fully recover the true positions of the stars with precision described by the Cramér-Rao Lower Bound[1]. While some undersampling can be tolerated without too much loss of astrometric precision, one should remember that moderation is a virtue. If the undersampling becomes severe enough that almost all of the light from a star falls within a single pixel, then the astrometric precision is significantly diminished[17].

The MPDY experiment has been based on simulated IRAC Ch1 observations. So how well does MPDY work with real IRAC Ch1 observations? Hoffmann's IRAC Ch1 intrapixel QE map was

based on Campaign Q focus observations[18] taken about 40 days after the launch of the *Spitzer Space Telescope*. The next obvious step in this research effort would be to analyze Campaign R data (taken 4 days later) with MPDY and determine just how well this theoretical approach works with real stellar near-infrared observations.

Mitigating the impact of flux loss problems seen in state-of-the-art NASA-grade infrared detectors is still in its early days. Hoffmann's IRAC Ch1 intrapixel QE map is the first attempt by the IRAC team to quantify this effect. Derivation of the intrapixel QE map is an *iterative process* due to the apparent centroid shifting caused by the non-uniform QE variation across a pixel; given an initial estimate of the intrapixel QE map, better positions of the input stellar images can then be determined, which, in turn, enables a better measurement of the intrapixel QE map to be made. Is a 5×5 map sufficiently fine enough to capture most of the PRF variations seen with IRAC Ch1? Would a 15×15 map be better or would that be overkill?

Much more work remains to be done. However, the possibility of significantly improving the precision and accuracy of space-based near-infrared stellar photometry and astrometry appears to be excellent. Ground-based infrared stellar photometry can typically achieve 10% accuracy and 5% accuracy under excellent conditions; the *Spitzer Space Telescope* is currently achieving only 5% photometry despite the fact that it is a cold stable observing platform in deep space. A significant improvement to 2-3% photometric accuracy might be possible with image analysis software that models the image formation process within the detector. A stretch goal of 1% photometric accuracy may even be achievable with *existing* space-based cameras using state-of-the-art infrared array detectors — if onboard cameras are electronically quiet and stable enough.

NASA and ESA astrophysical mission designers have a penchant to approve of optical designs that are undersampled. Although excellent justifications can often be made for using complex optical designs that have ugly Point Spread Functions (e.g., reduced total mission cost) or for using detectors that are too big at a given wavelength (e.g., giving a wider field-of-view), the analysis of resultant image data from these designs is frequently problematical. Reliance upon traditional ground-based image analysis codes may preclude the use of innovative space-based optical designs if such designs are rejected during the design review process for the very practical reason that there is no proven way to accurately analyze the resultant image data.

The better a telescope and its instrumentation are characterized, the better one can extract the full scientific potential out of the telescope/instrument combination. Enhancing the scientific return of NASA's existing Great Observatories does not come without a real cost; better characterization of space-based instrumentation may very likely require the development of new onboard calibration procedures. Some enhancements may be easy to achieve if the time spent doing the new calibrations can be folded into existing instrument calibration schedules. Other enhancements may simply not be practical – at this time – because current instruments may have electronic designs that are not quiet or stable enough to realize the enhancement. By learning from the good and bad engineering decisions that were made for existing astrophysical missions, we can enhance the scientific return of future astrophysical missions while possibly lowering total mission costs.

References

[1] *Stellar Photometry and Astrometry with Discrete Point Spread Functions*,
Mighell, K. J. 2005,
MNRAS, 361, 861–878

[2] FITS Support Office: `http://fits.gsfc.nasa.gov`

[3] MATPHOT web site: `http://www.noao.edu/staff/mighell/matphot/`

[4] *Accurate stellar photometry in crowded fields*,
Mighell, K. J. 1989,
MNRAS, 238, 807–833

[5] *Algorithms for CCD Stellar Photometry*,
Mighell, K. J. 1999,
in Astronomical Data Analysis Software and Systems VIII,
edited by D. M. Mehringer, R. L. Plante, and D. A. Roberts,
ASP Conference Series, Vol. 172., (ASP: San Francisco), 317–328

[6] *A Method for the Solution of Certain Problems in Least Squares*,
Levenberg, K. 1944,
Q. App. Math., 2, 164–168

[7] *An Algorithm for Least-Squares Estimation of Nonlinear Parameters*,
Marquardt, D. 1963,
J. SIAM, 11, 431–441

[8] *Innovative image analysis software as a technology driver for advances in space telescope design*,
Mighell, K. J. 2006,
in Space Telescopes and Instrumentation I: Optical, Infrared, and Millimeter,
edited by J. C. Mather, H. A. MacEwen, and M. W. de Graauw,
Proceedings of SPIE, Vol. 6265, pp. 62652T-1 to 62652T-12
`[preprint: http://www.noao.edu/staff/mighell/spie2006/mighellSPIE2006AS01.pdf]`

[9] *Analysis of K-band imaging of the wide binary system σ CrB with the Lick Observatory NGS AO system*,
Mighell, K. J. 2006,
in Advances in Adaptive Optics II,
edited by B. L. Ellerbroek and D. B. Calia,
Proceedings of SPIE, Vol. 6272, pp. 62720I-1 to 62720I-6
`[preprint: http://www.noao.edu/staff/mighell/spie2006/mighellSPIE2006AS08.pdf]`

[10] *Mitigating the Impact of Large Intrapixel Quantum Efficiency Variations on Precision Stellar Photometry and Astrometry*,
Mighell, K. J. 2005,
BAAS, 37, 1196 (poster #23.03, 207th AAS meeting, 2006 January 9, Washington D.C.)
`[abstract: http://www.aas.org/publications/baas/v37n4/aas207/637.htm]`

[11] *Infrared Array Camera Data Handbook (Version 3.0; January 20, 2006)*,
Reach, W. T., et al. 2006
[http://ssc.spitzer.caltech.edu/irac/dh/iracdatahandbook3.0.pdf]

[12] *Intra-pixel Variation Effect on Aperture Photometry*,
Hoffmann, B. 2005,
IRAC/TMo5-028 (Simfit Report 59; Version 2: December 10, 2005)

[13] *25 Position Model Pixel Repsonse Funcitons (PRF) Description and Quality*,
Hoffmann, B. 2005,
IRAC/TMo5-014 (Simfit Report 52; September 3, 2005)

[14] *The State of the focus and image quality of the Spitzer Space Telescope as measured in Orbit*,
Gehrz, R. D., et al. 2004,
in Optical, Infrared, and Millimeter Space Telescopes,
edited by J. C. Mather,
Proceedings of SPIE, Vol. 5487, 166–176

[15] *Accuracy of measurement of star images on a pixel array*,
King, I. R. 1983,
PASP, 95, 163–168

[16] *The Infrared Array Camera (IRAC) for the Spitzer Space Telescope*,
Fazio, G. G., et al. 2004,
ApJS, 154, 10–17

[17] *Cramér-Rao lower bounds on the performance of charge-coupled-device optical position e stimator*,
Winick, K. A. 1986,
JOSA A, 3, 1809–1815

[18] *Determination of Spitzer Space Telescope focus from IRAC images without a focus slew*,
Hoffmann, W. F., et al. 2004,
in Optical, Infrared, and Millimeter Space Telescopes,
edited by J. C. Mather,
Proceedings of SPIE, Vol. 5487, 186-200

Browse Publications

- Nanotechnology
- Defense & Security
- Aerospace, Remote Sensing, & Astronomy
- Automation, Inspection, & Product Engineering
- Biomedical Optics
- Communications & Fiber Optics
- Electronic Imaging, Displays, & Medical Imaging
- Lasers & Applications
- Microelectronics, Optoelectronics, & Micromachining
- Optical Physics, Chemistry, & Biology
- Optical Science & Engineering
- Signal & Image Processing

Abstract

PUBLICATIONS

Innovative image analysis software as a technology driver for advances in space telescope design

Kenneth J. Mighell

Publication: Proc. SPIE Vol. 6265, 62652T, Space Telescopes and Instrumentation I: Optical, Infrared, and Millimeter; John C. Mather, Howard A. MacEwen, Mattheus W. de Graauw; Eds.

Publication Date: Jul 2006

Abstract

Innovative image analysis software has the potential to act as a technology driver for advancing the state-of-the- art in the design of space telescopes and space-based instrumentation. Total mission costs can sometimes be significantly reduced by using innovative compact optical designs that create ugly Point Spread Functions. Most traditional astronomical image analysis techniques, like precision stellar photometry and astrometry, were developed for the analysis of ground-based image data and many photometric reduction codes cleverly take full advantage of the blurring caused by the Earth's atmosphere. Image data from space-based cameras, however, is typically characterized by having significant amounts of power at high spatial frequencies. Mission designers have a penchant to approve of optical designs that are undersampled. Although excellent justifications can often be made for using complex optical designs that have ugly Point Spread Functions (e.g., reduced total mission cost) or for using detectors that are too big at a given wavelength (e.g., giving a wider field-of-view), the analysis of resultant image data from these designs is frequently problematical. Reliance upon traditional ground-based image analysis codes may preclude the use of innovative space-based optical designs if such designs are rejected during the design review process for the very practical reason that there is no proven way to accurately analyze the resultant image data. I discuss ongoing research efforts to develop new image analysis algorithms specifically for space-based cameras that may help NASA and ESA to enhance the scientific returns from future astrophysical missions while possibly lowering total mission costs.

« Return to Search Results

"Innovative image analysis software as a technology driver for advances in space telescope design", Mighell, K. J. 2006, in *Space Telescopes and Instrumentation I: Optical, Infrared, and Millimeter*, edited by J. C. Mather, H. A. MacEwen, and M. W. de Graauw, Proc. SPIE Vol. 6265, pp. 62652T-1 to 62652T-12

Innovative Image Analysis Software as a Technology Driver for Advances in Space Telescope Design

Kenneth J. Mighell[a]

[a]National Optical Astronomy Observatory, 950 N. Cherry Ave., Tucson, AZ 85719, U.S.A.

ABSTRACT

Innovative image analysis software has the potential to act as a technology driver for advancing the state-of-the-art in the design of space telescopes and space-based instrumentation. Total mission costs can sometimes be significantly reduced by using innovative compact optical designs that create ugly Point Spread Functions. Most traditional astronomical image analysis techniques, like precision stellar photometry and astrometry, were developed for the analysis of ground-based image data and many photometric reduction codes cleverly take full advantage of the blurring caused by the Earths atmosphere. Image data from space-based cameras, however, is typically characterized by having significant amounts of power at high spatial frequencies. Mission designers have a penchant to approve of optical designs that are undersampled. Although excellent justifications can often be made for using complex optical designs that have ugly Point Spread Functions (e.g., reduced total mission cost) or for using detectors that are too big at a given wavelength (e.g., giving a wider field-of-view), the analysis of resultant image data from these designs is frequently problematical. Reliance upon traditional ground-based image analysis codes may preclude the use of innovative space-based optical designs if such designs are rejected during the design review process for the very practical reason that there is no proven way to accurately analyze the resultant image data. I discuss ongoing research efforts to develop new image analysis algorithms specifically for space-based cameras that may help NASA and ESA to enhance the scientific returns from future astrophysical missions while possibly lowering total mission costs.

Keywords: stellar photometry, astrometry, infrared detectors, Spitzer Space Telescope, IRAC, MATPHOT

1. CAN YOU FIT A BANANA?

Since the early 1990s, NASA's astrophysical mission designers have been challenged by administrators to do more science with fewer dollars. The "faster-better-cheaper" approach of mission design has lead to many innovative mission concepts which achieve lower total mission cost at the price of having some distortion in the optical design of instruments and/or telescopes. One way of compensating for distorted optics is to do more image processing with clever analysis algorithms.

Technology Readiness Level[1] (TRL) enhancement programs at NASA, like the *Applied Information Systems Research* (AISR) program of NASA's Science Mission Directorate, can significantly help NASA's astrophysical mission designers by promoting the development of new image processing algorithms from a basic technology research level (e.g., TRL 1–3) to the point where mission designers can consider using these new image processing algorithms in future NASA missions (e.g., TRL 5–6). Space-based demonstration of new technologies is clearly beyond the scope and means of the AISR program, yet AISR can develop new applied information systems technologies which would be excellent candidates for consideration for use in demonstrator programs like the *New Millennium Program*[2] (NMP) which tests advanced technology for use in space flight.

One of the early design concepts for the 8-m *Next Generation Space Telescope* (*NGST*), currently known as the 6.5-m *James Webb Space Telescope* (*JWST*), had a very elliptical primary mirror in order to fit it into a 4-m diameter launch shroud. John Mather, the NGST Project Scientist, described this concept to me at the 193rd meeting of the American Astronomical Society (AAS) in January 1999 in Austin, Texas. He explained that one of the problems associated with the elliptical primary mirror design was the fact that the oddly shaped primary mirror would cause stars to be shaped like bananas. He then asked me: "Can you fit a banana?" I replied: "Yes." Since there was as yet no clear consensus within the *NGST* project in 1999 whether accurate stellar photometry and astrometry was theoretically and/or practically possible with very complex Point Spread Functions (PSFs), he replied: "Prove it!"

Through funding provided by the AISR program, I have met Mather's challenge by demonstrating that precise and accurate stellar photometry and astrometry is possible and practical with ugly space-based PSFs which have high spatial frequencies rarely seen in ground-based astronomy due to the blurring of the Earth's atmosphere.

Section 2 describes the role of Point Response Functions (PRFs) in the image formation process. An information-theory based point-source photometric and astrometric performance model which can be used to measure the measurement efficiency of stellar photometric reduction codes is outlined in Section 3. The key features of my MATPHOT algorithm, for precision stellar photometry and astrometry with discrete (sampled) PSFs, are described in Section 4. Problems related to doing astrophysical imaging with ugly (imperfect) detectors with large intrapixel quantum efficiency (QE) variations is presented in Section 5. A practical example is given in Section 6 where a theoretical analysis indicates that the current 5% stellar photometry precision limit from Channel 1 of *Spitzer Space Telescope's* Infrared Array Camera (IRAC) may be significantly improved in the near future through better modeling of the image formation process within the detector. Concluding remarks are given in Section 7.

2. POINT RESPONSE FUNCTIONS

A Point Response Function (PRF), Ψ, is the convolution of a Point Spread Function (PSF), ϕ, and a Detector Response Function (DRF), Λ :

$$\Psi \equiv \phi * \Lambda \ . \tag{1}$$

The PSF describes the two-dimensional distribution of *photons* from a star *just above the detector.* Although stellar photons are distributed as a point source above the Earth's atmosphere, a stellar image becomes a two-dimensional distribution as the stellar photons are scattered by atmospheric turbulence. The blurred stellar image is then further degraded by passage of the stellar photons through the combined telescope and camera optical elements (such as mirrors, lenses, apertures, etc.). The PSF is the convolution of all these blurring effects on the original point-source stellar image. The DRF is a two-dimensional discrete (sampled) function that describes how the detector electronics convert stellar photons (γ) to electrons (e^-) — including such effects as the diffusion of electrons within the detector substrate or the reflection (absorption) of photons on (in) the gate structures of the detector electronics.

A perfect DRF gives a PRF that is a *sampled version* of the PSF:

$$\Psi_i \equiv \int_{x_i-0.5}^{x_i+0.5} \int_{y_i-0.5}^{y_i+0.5} \phi(x,y)\, dx\, dy \ , \tag{2}$$

where i^{th} pixel (px) of the PRF located at (x_i, y_i) is the volume integral of the PSF over the area of the i^{th} pixel. The actual limits of the above volume integral reflect the appropriate mapping transformation of the x and y coordinates onto the CCD pixel coordinate system.

The sharpness of a PRF is defined as the volume integral of the *square* of the *normalized* PRF:

$$\text{sharpness} \equiv \iint_{-\infty}^{+\infty} \tilde{\Psi}^2 \, dx\, dy \ \equiv \iint_{-\infty}^{+\infty} \left(\frac{\Psi}{\text{V}}\right)^2 \, dx\, dy \ , \tag{3}$$

where V is the volume integral of the PRF, which has a value between one and zero. Physically, sharpness is a shape parameter which describes the "pointiness" of a PRF; sharpness values range from a maximum of one (all of the stellar flux is found within a single pixel) to a minimum of zero (a flat stellar image). For example, cameras that are out of focus have broad PSFs with sharpness values near zero. A normalized Gaussian[3] PSF with a standard deviation of $\mathcal{S}$ pixels that has been *oversampled* with a perfect DRF will have a sharpness value of $1/4\pi\mathcal{S}^2$. A critically-sampled normalized Gaussian PRF has a sharpness of $1/(4\pi)$ and any PRF with a sharpness value greater than that value ($\sim$0.0796) can be described as being undersampled. Diffraction limited optics, theoretically, give sharpness values that decrease (i.e., PSFs become flatter) with increasing photon wavelength – for a fixed pixel (detector) size. With real astronomical cameras, the value of sharpness frequently depends on *where the center of a star is located within the central CCD pixel* of the stellar image. For example, the *Hubble*

Space Telescope (HST) WFPC2 Planetary Camera PRF at a wavelength of 200 nm has an observed sharpness value of 0.084 if the PRF is centered in the middle of a PC pixel or 0.063 if the PRF is centered on a pixel corner (Table 6.5 of Ref. 4); at 600 nm the observed sharpness values range from 0.066 (pixel-centered) to 0.054 (corner-centered). The Wide-Field Cameras of the *HST* WFPC2 instrument have pixels which are approximately half the angular resolution of the PC camera pixels; stellar images on the WF cameras are undersampled and the observed range of WF camera sharpness values are 0.102–0.120 at 200 nm and 0.098–0.128 at 600 nm.

The *effective-background area*, $\boldsymbol{\beta}$, of a PRF is defined as the *reciprocal* of the volume integral of the *square* of the PRF. Alternatively, the effective-background area (a.k.a. *equivalent-noise area*[5] or *effective solid angle*) of a PRF is equal to the reciprocal of the product of its sharpness and the square of its volume:

$$\boldsymbol{\beta} \equiv \left[\iint_{-\infty}^{+\infty} \Psi^2 \, dx \, dy \right]^{-1} = \frac{1}{\mathrm{V}^2 \, \mathsf{sharpness}} \, . \tag{4}$$

The effective-background area of a normalized Gaussian PRF is $4\pi\mathcal{S}^2$ px, where $\mathcal{S}$ is the standard deviation in pixels; a critically-sampled normalized Gaussian PRF has an effective-background area of $4\pi \approx 12.57$ px. King[5] notes that numerical integration of a realistic ground-based stellar profile gives an effective-background area of $30.8\,\mathcal{S}^2$ instead of the value of $4\pi\,\mathcal{S}^2$ for a normalized Gaussian profile.

3. PHOTOMETRIC AND ASTROMETRIC PERFORMANCE MODEL

Consider a CCD observation of single isolated star on a flat sky background. Assuming one already knows the PRF of the observation at the location of the star, a simple model of the observation would have just two parameters: the stellar intensity ($\mathcal{E}$) in electrons, and the observed background sky level ($\mathcal{B}$) in electrons. The observational model for the i^{th} pixel would be

$$m_i \equiv \mathcal{B} + \mathcal{E}\mathrm{V}\tilde{\Psi}_i \, , \tag{5}$$

where V is the volume integral of the PRF and $\tilde{\Psi}_i$ is the value of the i^{th} pixel of the *normalized* PRF ($\tilde{\Psi}_i \equiv \Psi_i/\mathrm{V}$).

I have developed a realistic point-source photometric performance model for CCD PSF-fitting stellar photometric reduction codes.[6] The theoretical *upper limit* for the photometric signal-to-noise ratio (S/N) of CCD PSF-fitting stellar photometric algorithms is

$$\mathsf{S/N} \equiv \frac{\mathcal{E}}{\sigma_{\mathcal{E}}} \approx \frac{\mathcal{E}}{\sqrt{\dfrac{\mathcal{E}}{\mathrm{V}} + \boldsymbol{\beta}\left(1 + \sqrt{\boldsymbol{\beta}/N}\right)^2 \left[\mathcal{B} + \sigma_{\mathrm{RON}}^2\right]}} \, , \tag{6}$$

where $\boldsymbol{\beta}$ is the effective-background area of the PRF and σ_{RON} is the rms CCD readout noise. These approximations assume, for the sake of simplicity, that any noise contribution due to dark current and quantization noise is negligible. While these additional noise sources can be added to create an even more realistic performance model for stellar photometry, the assumption of low dark current and minimal quantization noise is realistic for state-of-the-art astronomical-grade CCD imagers. This photometric performance model has bright and faint star limits[6] which are the same, respectively, as the bright and faint star Cramér-Rao Lower Bounds for stellar photometry imaged with a perfect noiseless detector.[5,7] The resulting photometric error is approximately

$$\Delta\mathsf{mag} \approx \frac{1.0857}{\mathsf{S/N}} \, , \tag{7}$$

where the constant 1.0857 is an approximation for Pogson's[8] ratio $a \equiv 5/\ln(100) = 2.5\log(e)$.

I have developed a realistic point-source astrometric performance model for CCD PSF-fitting stellar photometric reduction codes.[6] The theoretical *lower limit* of the rms measurement error for the stellar position in the x coordinate ($\mathcal{X}$) for a single isolated star on a flat sky is

$$\sigma_{\mathcal{X}} \approx \sqrt{\frac{\mathcal{L}^2}{\mathcal{E}\mathrm{V}} \left[1 + 8\pi\left(\mathcal{B} + \sigma_{\mathrm{RON}}^2\right)\frac{\mathcal{L}^2}{\mathcal{E}\mathrm{V}}\right]} \, , \tag{8}$$

where

$$\mathcal{L} \equiv \sqrt{\frac{\boldsymbol{\beta}\,\mathrm{V}^2}{4\pi}} \;=\; \frac{1}{\sqrt{4\pi\;\mathsf{sharpness}}} \tag{9}$$

is the *critical-sampling scale length* of the PRF* in pixel units. The rms stellar position measurement error in the y coordinate ($\mathcal{Y}$) is the same, by symmetry, as for $\mathcal{X}$: $\sigma_{\mathcal{Y}} = \sigma_{\mathcal{X}}$. The critical-sampling scale length of a critically-sampled PRF imaged with a perfect detector, be definition, is one pixel; $\mathcal{L} > 1$ indicates that the PRF is *oversampled*, while $\mathcal{L} < 1$ indicates that the PRF is *undersampled*.

This astrometric performance model has bright and faint star limits[6] which are the same, respectively, as the bright and faint star Cramér-Rao Lower Bounds for stellar astrometry of a single isolated Gaussian star on a flat sky background imaged with a perfect noiseless detector with infinitely small pixels (a.k.a. the *photonic* limit).[7] The Cramér-Rao Lower Bound for stellar astrometry of a single isolated Gaussian star on a flat sky background imaged with a perfect noiseless CCD *with square pixels*[9] quickly approaches the photonic limits with *well-sampled* observations; undersampled observations will have larger astrometric errors than predicted by the photonic limits.

4. PHOTOMETRY & ASTROMETRY WITH DISCRETE PSFS

I have developed a C-language implementation[10] of my MATPHOT algorithm[6,11,12] for precise and accurate stellar photometry and astrometry with discrete Point Spread Functions (PSFs). The MATPHOT code uses discrete (sampled) Point Spread Functions consisting of a numerical table represented by a matrix in the form of a FITS[13] image. Discrete PSFs are shifted within an observational model using a 21-pixel-wide damped sinc function,

$$f^{\mathrm{shifted}}(x_0) \equiv \sum_{i=-10}^{10} f(x_i) \frac{\sin\left(\pi(x_i - x_0)\right)}{\pi(x_i - x_0)} \exp\left(-\left[\frac{x_i - x_0}{3.25}\right]^2\right) , \tag{10}$$

and position partial derivatives are computed using a five-point numerical differentiation formula,

$$f\,'(x_i) \approx \frac{1}{12}\left[f(x_{i-2}) - 8\,f(x_{i-1}) + 8\,f(x_{i+1}) - f(x_{i+2})\right] . \tag{11}$$

Precise and accurate stellar photometry and astrometry are achieved with undersampled CCD observations by using supersampled discrete PSFs that are sampled 2, 3, or more times more finely than the observational data. Although these numerical techniques are not mathematically perfect, they are sufficiently accurate for precision stellar photometry and astrometry due to photon noise which is present in all astronomical imaging observations.[6] The current implementation[10] of the MATPHOT algorithm is based on a robust implementation[11,14] of the Levenberg[15]-Marquardt[16] method of nonlinear least-squares minimization. Detailed analysis of simulated *Next Generation Space Telescope* (*NGST*) observations demonstrate that millipixel relative astrometry and millimag photometric precision is achievable with complicated space-based discrete PSFs.[6]

A simulated *NGST* V-band stellar observation with the 8-meter TRW-concept 1.5-micron diffraction-limited primary mirror is shown in Fig. 1 with the 90%, 50%, 10%, 1%, and 0.1% contours relative to the peak intensity. The pixel scale is 0.0128 arcsec pixel^{-1}. The original version of this PSF was kindly provided by John Krist (STScI, now at JPL). The right side of Fig. 1 shows the MATPHOT-based analysis of 10,000 simulated *NGST V*-band CCD observations of stars with true flux values between 250 and 10^6 electrons (photons). Each observation was simulated with a 2×2 supersampled *NGST* PSF located near the center of 60×60 pixels on a flat background of 100 electrons (e^-) with a CCD readout noise level of 3 e^- pixel^{-1}. The results are plotted using box-and-whisker plots[6] to better display the statistical range of recovered values for photometry and astrometry. Fig. 2 shows similar results for simulated 6.5-m *James Webb Space Telescope* (*JWST*) observations with a perfect one-micron PSF (shown with a log stretch to better display the higher spatial frequencies). The solid curves in Figs. 1 and 2 show the predicted median performance of the MATPHOT algorithm for these simulations;

*From the definition of the effective-background area of an oversampled Gaussian PRF with a standard deviation of $\mathcal{S}$ pixels and $\mathrm{V}<1$, $\boldsymbol{\beta}_{\mathsf{G}} \equiv 4\pi\mathcal{S}^2/\mathrm{V}^2$, one sees that critical-sampling scale length has been designed to be a proxy for $\mathcal{S}$ for *any* PRF.

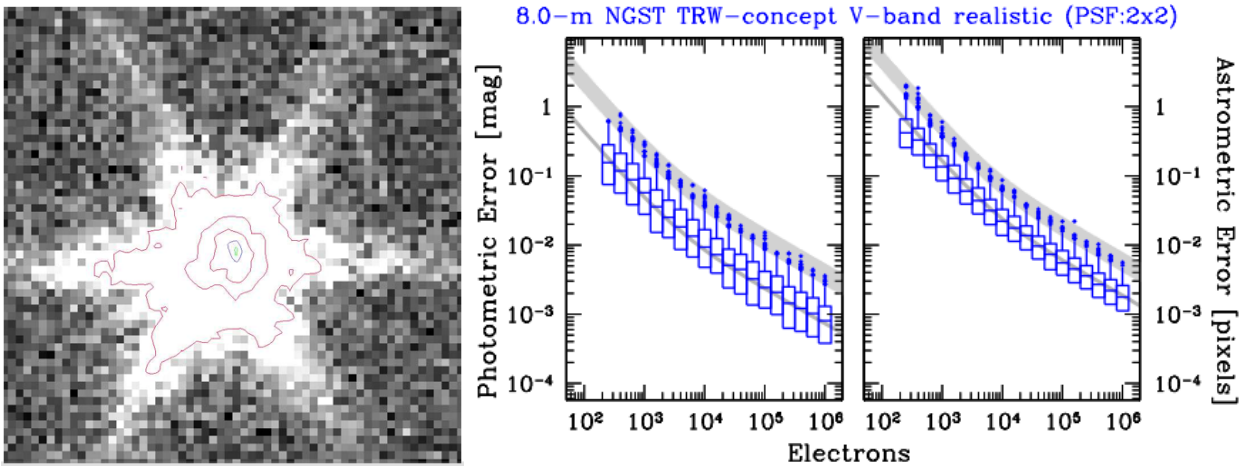

Figure 1. MATPHOT analysis of 10,000 simulated *NGST* stellar observations.

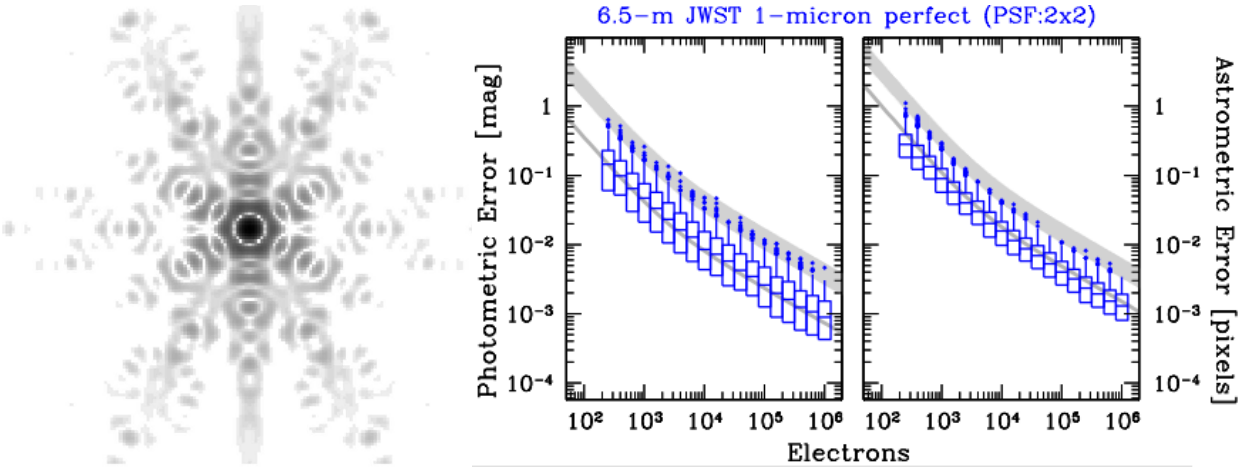

Figure 2. MATPHOT analysis of 10,000 simulated *JWST* stellar observations.

note that the actual median values (central bars in the boxes) lie on top or very near the performance model prediction. The wide bands in the above photometric (astrometric) error plots show the predicted outlier region for 2.3σ (3.0σ) to 5.0σ outliers (shown as points above the top whisker in Figs. 1 and 2). Note how well the theoretical performance model agrees with the actual MATPHOT measurements — even with these very complicated (simulated) space-based discrete PSFs.

5. UGLY DETECTORS

Current infrared detector technology can produce imagers with non-uniform pixel response functions. Lauer[17] reported peak-to-peak variation of 0.39 mag at the J band (F110W) and 0.22 mag at H band (F160W) of the NIC3 camera of the *HST* NICMOS instrument. The peak-to-peak variation of 0.2 mag at F160W with NIC3 has been independently verified.[18] Significant flux loss due to non-uniform intrapixel pixel response functions is clearly an observational fact in some existing space-based astronomical cameras.

An experimental version of the MATPHOT demonstrator program, called MPDX,[6] was created to simulate such an IR detector; a pixel was split into 16 subpixels and all the subpixels in the first row and column were declared to be gate structures with zero efficiency converting photons to electrons and the other nine subpixels had 100% conversion efficiency. Note that only 56% of the total pixel area was optically active.

Ten thousand undersampled CCD stellar observations of −15 mag stars (10^6 electrons) were simulated and analyzed with MPDX using a 4×4 supersampled version of the simulated V-band *NGST* PSF described above.

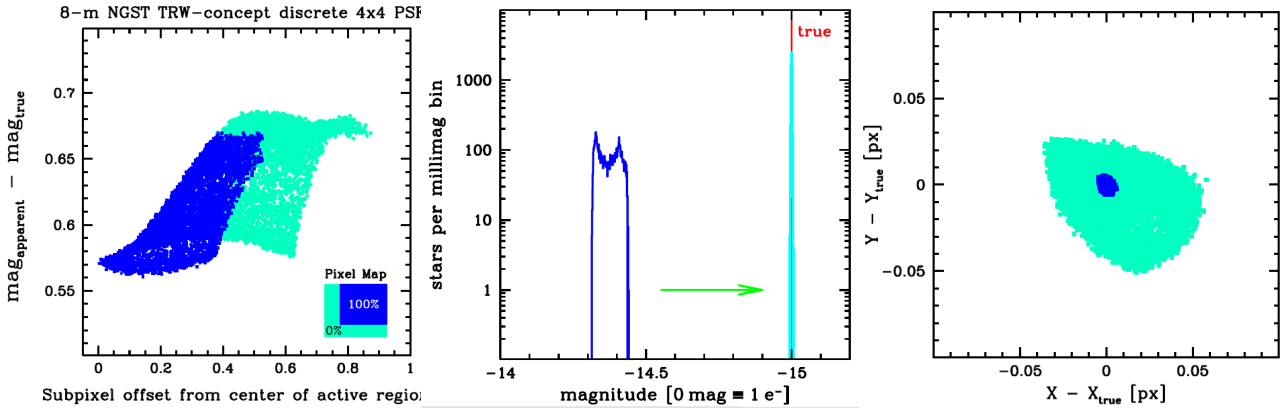

Figure 3. Results of the MPDX experiment with simulated *NGST* observations.

The optically inactive gate structures of the pixel cause the observed number of electrons in each stellar image to be significantly less than the number of photons which fell on the detector. *The total amount of loss was dependent on where the center of the star fell within the central pixel of the stellar image.* The left side of Fig. 3 shows that stars centered in the middle of the active area of a pixel suffered a ∼40% loss ($\Delta m \approx 0.56$ mag) while those centered on gate structures lost up to 47% ($\Delta m \approx 0.69$ mag).[6]

The mean *apparent* (observed) stellar magnitude for these −15 mag stars was -14.3723 ± 0.0354 mag. The photometric performance model predicts an rms measurement error of 0.0015 mag for these bright stars. With an average loss of 44% and an rms measurement error that is *more than 23 times larger* than expected from photon statistics, *the observed stellar magnitudes were neither precise or accurate* (see the left histogram of the central graph in Fig. 3).

The mean *measured* stellar magnitude reported by MPDX was -14.9999 ± 0.0015 mag and the mean rms error estimated by the program was 0.001503 ± 0.000016 mag (see the right histogram of the central graph of Fig. 3). The photometric performance of the experimental version of MATPHOT is fully consistent with theoretical expectations — which were derived[6] for an ideal detector with no intrapixel QE variation.

The experimental version of MATPHOT was able to do an excellent job in recovering the true stellar magnitude of the 10,000 −15 mag stars — despite being presented with a worst-case scenario of undersampled observations with an ugly PSF imaged on an ugly detector with a very large intrapixel QE variation .[6]

Non-uniform intrapixel response functions can also affect astrometric (position) measurements. Photons that are not converted to electrons can cause the apparent intensity weighted centroid of the PRF (i.e., the recorded stellar image) to be in a different location than the intensity weighted centroid of the PSF (i.e., the photon distribution function just above the detector). The right graph of Fig. 3 demonstrates this problem; the light grey (cyan) points show the large systematic astrometric errors of the *apparent* centroid (intensity weighted mean) of the stellar image; the black (blue) points show the small *random* astrometric errors of the MPDX measurements. In this particular experiment, the Fig. 3 indicates that the apparent position of the stellar image may in fact be several hundredths of a pixel off from the true location of the PSF – this is a very large systematic error considering that the expected position error from photon statistics is only 1.7 millipixels.

The experimental version of MATPHOT was able to do an excellent job in recovering the true stellar position of the 10,000 −15 mag stars — despite the fact that the apparent positions of Point Response Functions were corrupted by the inactive gate structures.

Excellent stellar photometry and astrometry is possible with ugly PSFs imaged onto ugly detectors as long as the image formation process within the detector *is accurately modeled by the photometric reduction code.*

6. SPITZER SPACE TELESCOPE'S INFRARED ARRAY CAMERA

The following is an extract from the IRAC Data Handbook:[19]

> The flux density of a point source measured from IRAC images depends on the exact location where the peak of the Point Response Function (PRF) falls on a pixel. This effect is due to the variations in the quantum efficiency of a pixel, and combined with the undersampling of the PRF, it is most severe in channel 1. The correction can be as much as 4% peak to peak. The effect is graphically shown in Figure 5.1 where the normalized measured flux density (y-axis) is plotted against the distance of the source centroid from the center of a pixel. The correction for channel 1 can be calculated from
>
> $$Correction = 1 + 0.0535 \times \left[\frac{1}{\sqrt{2\pi}} - p \right] \tag{5.14}$$
>
> where p is the pixel phase ($p = \sqrt{(x - x_0)^2 + (y - y_0)^2}$), where x, y, is the centroid of the point source and x_0 and y_0 are the integer pixel numbers containing the source centroid. The correction was derived from photometry of a sample of stars, each star observed at many positions on the array. The "ratio" on the vertical axis in Figure 5.1 is the ratio of the measured flux density to the mean value for the star. To correct the flux of a point source, calculate the correction from Equation 5.14 and divide the source flux by that correction. Thus, the flux of sources well-centered in a pixel will be reduced by 2.1%. Pixel phase corrections for other channels, if necessary, and after they have been more accurately determined than currently, will be given in future Data Handbook versions.

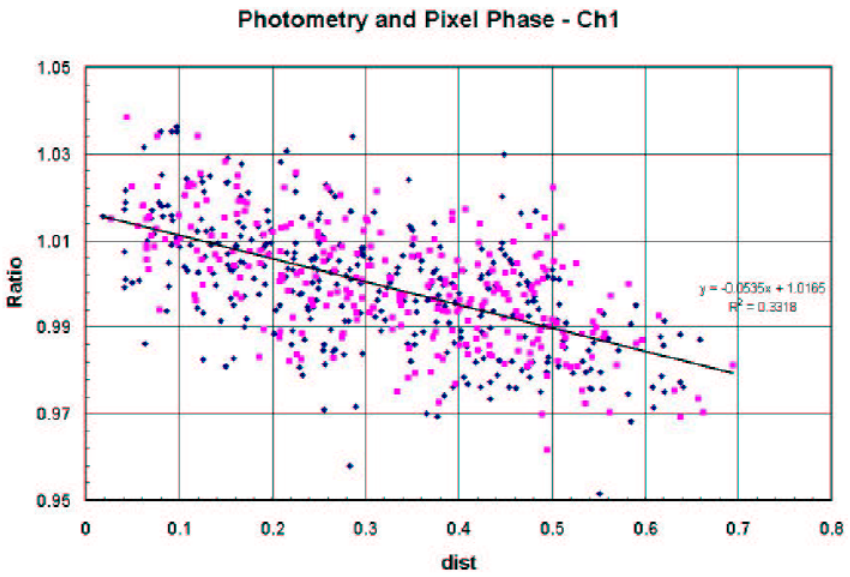

Figure 5.1: Dependence of point source photometry on the distance of the centroid of a point source from the nearest pixel center in channel 1. The ratio on the vertical axis is the measured flux density to the mean value for the star, and the quantity on the horizontal axis is the fractional distance of the centroid from the nearest pixel center.

Following discussions with *Spitzer Space Telescope*'s Infrared Array Camera (IRAC) team members at the 207th meeting of the AAS in January 2006 in Washington, D.C., I have started working with various IRAC team members with the goal of determining if it might be possible to improve stellar photometry from IRAC's Channel 1 (3.6μ) by creating an experimental version of the existing MATPHOT code with an effective intrapixel quantum efficiency map for IRAC Ch1 hard-wired into the code.

Bill Hoffmann, an IRAC team member at the University of Arizona, has recently made the first estimate of the intrapixel QE variation across a single IRAC Channel 1 pixel:

$$\text{intrapix} = \begin{pmatrix} 0.813 & 0.875 & 0.875 & 0.875 & 0.813 \\ 0.875 & 1.000 & 1.000 & 1.000 & 0.875 \\ 0.875 & 1.000 & 1.000 & 1.000 & 0.875 \\ 0.875 & 1.000 & 1.000 & 1.000 & 0.875 \\ 0.813 & 0.875 & 0.875 & 0.875 & 0.813 \end{pmatrix} .$$

The mean conversion efficiency of this 5×5 convolution matrix is 91.01% . This is actually the *relative* intrapixel QE map since the central subpixels of this map were arbitrarily set to one; while the quantum efficiency of IRAC Channel 1 is high, the actual *absolute* values for the central subpixels are likely to be less than one. Full details about the derivation of this intrapixel quantum efficiency map may be found in Hoffmann's report *Intra-pixel Variation Effect on Aperture Photometry.*[20]

Hoffmann[21] has computed theoretical 5×5 supersampled versions of the IRAC Ch1 PSF across the camera's field-of-view. Fig. 4 shows the model PSF which was computed for the central region of the IRAC Ch1. The left side of Fig. 4 shows a linear stretch of the PSF and the right side shows a log stretch. Although the PSF appears to be reasonable in the linear stretch, which emphasizes the bright central core, the log stretch shows the numerous weak higher-spatial-frequency features of this very complicated PSF. IRAC Ch1 PSFs are significantly undersampled by the IRAC Ch1 camera;[22] the mean effective background area[6] (a.k.a. equivalent noise area[5]) is 7.0 pixels[23] as compared to the canonical value of 4π (∼12.6 pixels) for a critically-sampled Gaussian PSF.

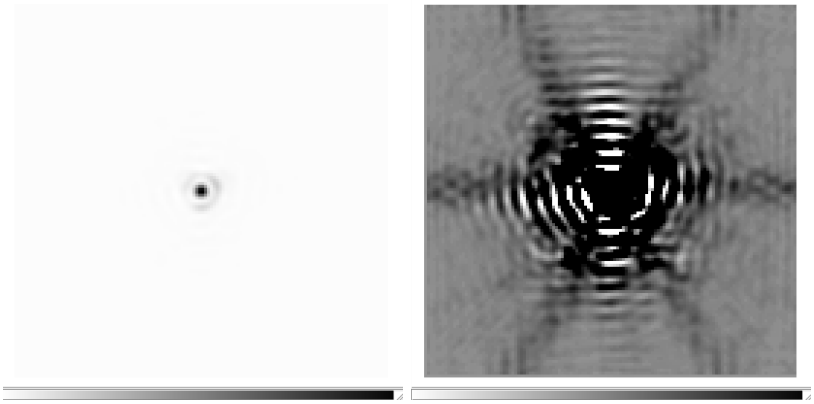

Figure 4. A theoretical 5×5 supersampled version of the IRAC Ch1 PSF.

Engineering decisions can significantly affect the science return of an instrument. The significant flux loss of IRAC Channel 1 is due to the combination of the non-negligible QE variation within a single pixel *and* the significant undersampling of the PSF by large (1.2 arcsec) pixels. The significant loss of flux in IRAC Ch1 could have been mitigated by simply oversampling the PSF. This capability was part of the initially proposed IRAC design which included both diffraction-limited and wide-field modes. The diffraction-limited mode was lost when the camera was simplified to include only the wide-field mode.

Image analysis software, which properly models the image formation process within the detector, has the *potential* of recovering the stellar flux lost by IRAC Ch1. Use of such software could thus enhance the science return from stellar (point source) observations which would appear, at first glance, to be limited to no better than 5% accuracy.

If an IRAC Ch1 observer follows the advice of the Infrared Array Camera Data Handbook[19] and uses the suggested correction formula (given above) to compensate for the lost stellar flux, then there will remain a variation of about 2% which is due to the fact that much of the *vertical variation seen in Fig. 5.1 of the IRAC Data Handbook is systematic* rather than random; the true flux correction function is a complicated two-dimensional distribution that is not circularly symmetric.

In a collaborative research effort with Bill Glaccum (Spitzer Science Center), Bill Hoffmann, and other IRAC team members, I have succeeded in creating a new experimental version of MATPHOT, called MPDY, which uses Hoffmann's intrapixel QE variation map[20] and the theoretical 5×5 supersampled PSF shown in Fig. 4 to create and analyze realistic IRAC Ch1 simulated observations.

Ten thousand IRAC Ch1 observations of a single star on a flat background were simulated and analyzed with MPDY. Each stellar observation was simulated using the theoretical 5×5 supersampled IRAC Ch1 PSF shown in Fig. 4; a star with 10^5 electrons was located near the center of 60×60 pixels on a flat background of 100 electrons (e^-). The efficiency of the photon to electron conversion process is calculated using the Hoffmann intrapixel QE map given above. Realistically noisy data was created by adding photon noise and a readout noise level of 3 e^- $pixel^{-1}$. Fig. 5 shows some of the results of the MPDY analysis of these simulations.

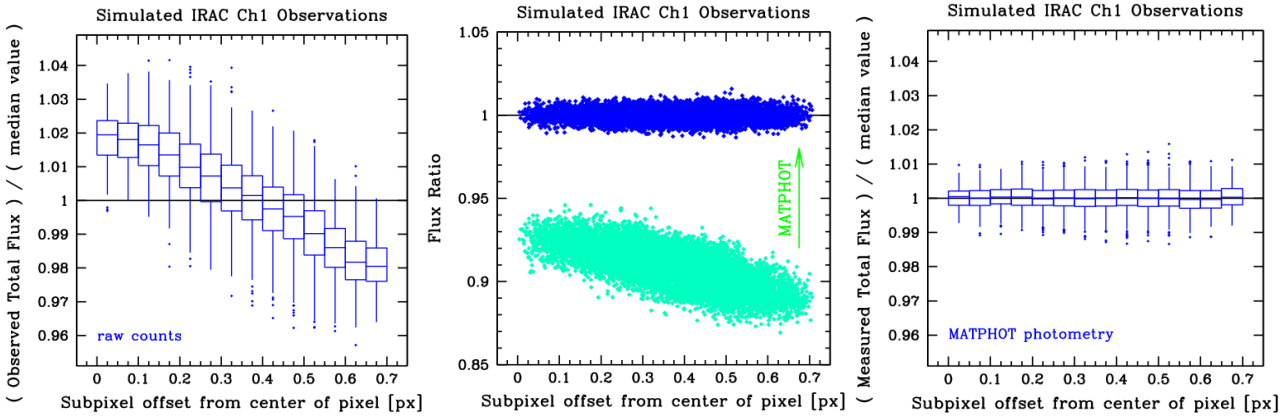

Figure 5. Results of the MPDY experiment with simulated IRAC Ch1 observations.

The horizontal axis of the left graph of Fig. 5 shows the subpixel offset (distance) the center of a star is from the middle of a pixel; stars centered near the middle of a pixel will have small offset values while stars located near the corner of a pixel will have offsets near 0.7 px. The vertical axis shows the *observed* (apparent) total flux divided by the *median observed* total flux value (90825.8 electrons, expected 100000) of all ten thousand stars. The median values of the box-and-whisker plots range from an excess flux of about 2% for stars centered near the center of a pixel to a flux deficit of about 2% for stars centered near the corner of a pixel. Note that this graph reproduces almost exactly the observed flux loss distribution seen in Fig. 5.1 of the IRAC Data Handbook.[19]

The vertical axis of the central graph of Fig. 5 shows the absolute flux ratio of the total fluxes divided by the true flux of 10^5 electrons. The light grey (cyan) points show the *observed* absolute flux ratios and the black (blue) points show the *measured* absolute flux ratios as reported by MPDY. Note that while the average stellar observation suffered an absolute flux loss of ∼9%, stars centered near the middle of a pixel suffered, on average, an absolute flux loss of ∼7% as compared to an absolute flux loss of ∼11% for stars centered near a pixel corner. It is important to note that the vertical scatter seen in the observed flux ratios (absolute or relative) is not random but systematic; a simple radial correction function can only partially recover the lost flux. The measured absolute flux ratios are clustered around unity and are not a function of subpixel offset; the vertical scatter seen in the measured absolute flux ratios is random. By modeling the image formation process within the detector, MPDY was able fully recover all of the stellar flux lost due to the non-uniform IRAC Ch1 intrapixel quantum efficiency variations.

The vertical axis of the right graph of Fig. 5 shows the *measured* total flux (as reported by MPDY) divided by the *median measured* total flux value (99972.3 electrons, expected 100000) of all ten thousand stars. This graph

shows that MPDY is able to recover the true stellar flux all the way down to the photon limit (photometric error of ∼3.9 millimag).

The previous section showed how non-uniform intrapixel QE maps can potentially cause significant systematic astrometric (position) errors for bright stars. Would we expect the IRAC Ch1 QE map to create systematic astrometric errors? Yes, indeed. If an intrapixel QE map is roughly circularly symmetric about the middle of a pixel (as is apparently the case for IRAC Ch1), then the centroid of an observed stellar image (i.e., the PRF) *which is centered in the middle of a pixel* will be approximately at the same position as the centroid of the PSF. However, if there is significant flux loss near the edges or corner of a pixel (as is apparently the case for IRAC Ch1), then the *centroid of a PRF which is centered near a pixel corner will most likely not be the same as the centroid of the PSF* — and the difference will be a systematic error rather than a random error.

The major component of the systematic astrometric error is the undersampling of the PSF by IRAC Ch1. The intrapixel QE variation in the detector just makes the matter a little worse. Naively doing centroiding on the recorded undersampled stellar image may lead to astrometry which has dubious value. However, photometric reduction codes that model the image formation process within the detector can fully recover the true positions of the stars with precision described by the Cramér-Rao Lower Bound. While some undersampling can be tolerated without too much loss of astrometric precsion, one should remember that moderation is a virtue. If the undersampling becomes severe enough that almost all of the light from a star falls within a single pixel, then the astrometric precsion is significantly diminished.[9]

The MPDY experiment has been based on simulated IRAC Ch1 observations. So how well does MPDY work with real IRAC Ch1 observations? Hoffmann's IRAC Ch1 intrapixel QE map was based on Campaign Q focus observations[24] taken about 40 days after the launch of the *Spitzer Space Telescope*. The next obvious step in this research effort would be to analyze Campaign R data (taken 4 days later) with MPDY and determine just how well this theoretical approach works with real stellar near-infrared observations.

Mitigating the impact of flux loss problems seen in state-of-the-art NASA-grade infrared detectors is still in its early days. Hoffmann's IRAC Ch1 intrapixel QE map is the first attempt by the IRAC team to quantify this effect. Derivation of the intrapixel QE map is an *iterative process* due to the apparent centroid shifting caused by the non-uniform QE variation across a pixel; given an initial estimate of the intrapixel QE map, better positions of the input stellar images can then be determined, which, in turn, enables a better measurement of the intrapixel QE map to be made. Is a 5×5 map sufficiently fine enough to capture most of the PRF variations seen with IRAC Ch1? Would a 15×15 map be better or would that be overkill?

Much more work remains to be done. However, the possibility of significantly improving the precision and accuracy of space-based near-infrared stellar photometry and astrometry appears to be excellent. Ground-based infrared stellar photometry can typically achieve 10% accuracy and 5% accuracy under excellent conditions; the *Spitzer Space Telescope* is currently achieving only 5% photometry despite the fact that it is a cold stable observing platform in deep space. A significant improvement to 2-3% photometric accuracy might be possible with image analysis software that models the image formation process within the detector. A stretch goal of 1% photometric accuracy may even be achievable with *existing* space-based cameras using state-of-the-art infrared array detectors — if onboard cameras are electronically quiet and stable enough.

7. CONCLUSION

NASA and ESA astrophysical mission designers have a penchant to approve of optical designs that are undersampled. Although excellent justifications can often be made for using complex optical designs that have ugly Point Spread Functions (e.g., reduced total mission cost) or for using detectors that are too big at a given wavelength (e.g., giving a wider field-of-view), the analysis of resultant image data from these designs is frequently problematical. Reliance upon traditional ground-based image analysis codes may preclude the use of innovative space-based optical designs if such designs are rejected during the design review process for the very practical reason that there is no proven way to accurately analyze the resultant image data.

The better a telescope and its instrumentation are characterized, the better one can extract the full scientific potential out of the telescope/instrument combination. Enhancing the scientific return of NASA's existing Great Observatories does not come without a real cost; better characterization of space-based instrumentation may

very likely require the development of new onboard calibration procedures. Some enhancements may be easy to achieve if the time spent doing the new calibrations can be folded into existing instrument calibration schedules. Other enhancements may simply not be practical – at this time – because current instruments may have electronic designs that are not quiet or stable enough to realize the enhancement. By learning from the good and bad engineering decisions that were made for existing astrophysical missions, we can enhance the scientific return of future astrophysical missions while possibly lowering total mission costs.

I hope that I have demonstrated that innovative image analysis software has great potential to act as a technology driver for advancing the state-of-the-art in the design of space telescopes and space-based instrumentation.

ACKNOWLEDGMENTS

I wish to thank Bill Hoffmann, Bill Glaccum, and the rest of the IRAC team for their support of this research effort which would not have been possible without the generous access they provided to previously proprietary data and reports. This work has been supported by a grant from the National Aeronautics and Space Administration (NASA), Interagency Order No. NNG05EB61I, which was awarded by the Applied Information Systems Research (AISR) Program of NASA's Science Mission Directorate.

REFERENCES

1. Technology Readiness Level Descriptions: `http://nmp.jpl.nasa.gov/st8-lib/NMP-TRL-Descriptions.pdf` .
2. New Millenium Program website: `http://nmp.nasa.gov` .
3. I. R. King, "The profile of a star image," *PASP* **83**, pp. 199–201, 1971.
4. J. Biretta, et al., *WFPC2 Instrument Handbook (Version 6.0)*, STScI, Baltimore, 2001.
5. I. R. King, "Accuracy of measurement of star images on a pixel array," *PASP* **95**, pp. 163–168, 1983.
6. K. J. Mighell, "Stellar photometry and astrometry with discrete point spread functions," *MNRAS* **362**, pp. 861–878, 2005.
7. M. J. Irwin, "Automatic analysis of crowded fields," *MNRAS* **214**, pp. 575–604, 1985.
8. N. Pogson, "Magnitudes of thirty-six of the minor planets for the first day of each month of the year 1857," *MNRAS* **17**, pp. 12–15, 1856.
9. K. A. Winick, "Cramér-Rao lower bounds on the performance of charge-coubled-device optical position estimator," *JOSA A* **3**, pp. 1809–1815, 1986.
10. MATPHOT web site: `http://www.noao.edu/staff/mighell/matphot` .
11. K. J. Mighell, "Algorithms for CCD stellar photometry," in *Astronomical Data Analysis Software and Systems VIII*, D. M. Mehringer, R. L. Plante, and D. A. Roberts, eds., *ASP Conference Series* **172**, pp. 317–328, 1999.
12. K. J. Mighell, "The MATPHOT algorithm for digital point spread function CCD stellar photometry," in *Astronomical Data Analysis II*, J.-L. Starck and F. D. Murtagh, eds., *Proc. SPIE* **4847**, pp. 207–216, 2002.
13. FITS Support Office web site: `http://fits.gsfc.nasa.gov` .
14. K. J. Mighell, "Accurate stellar photometry in crowded fields," *MNRAS* **238**, pp. 807–833, 1989.
15. K. Levenberg, "A method for the solution of certain problems in least squares," *Quarterly of Applied Mathematics* **2**, pp. 164–168, 1944.
16. D. Marquardt, "An algorithm for least-squares estimation of nonlinear parameters," *SIAM Journal of Applied Mathematics* **11**, pp. 431–441, 1963.
17. T. R. Lauer, "The photometry of undersampled point-spread functions," *PASP* **111**, pp. 1434–1443, 1999.
18. R. N. Hook and A. S. Fruchter, "Dithering, sampling and image reconstruction," in *Astronomical Data Analysis Software and Systems IX*, N. Manset, C. Veillet, and D. Crabtree, eds., *ASP Conference Series* **216**, pp. 521–530, 2000.
19. W. T. Reach, et al., *Infrared Array Camera Data Handbook (Version 3.0; January 20, 2006)*, `[http://ssc.spitzer.caltech.edu/irac/dh/iracdatahandbook3.0.pdf]`, 2006.
20. B. Hoffmann, "Intra-pixel variation effect on aperture photometry," IRAC/TMo5-028 (Simfit Report 59; Version 2: December 10, 2005), 2005.

21. B. Hoffmann, "25 position model pixel response functions (prf) description and quality," IRAC/TMo5-014 (Simfit Report 52 Final), 2005.
22. R. D. Gehrz, et al., "The state of the focus and image quality of the Spitzer Space Telescope as measured in orbit," in *Optical, Infrared, and Millimeter Space Telescopes*, J. Mather, ed., *Proc. SPIE* **5487**, pp. 166–176, 2004.
23. G. G. Fazio, et al., "The Infrared Array Camera (IRAC) for the Spitzer Space Telescope," *APJS* **154**, pp. 10–17, Sept. 2004.
24. W. F. Hoffmann, et al., "Determination of Spitzer Space Telescope focus from irac images without a focus slew," in *Optical, Infrared, and Millimeter Space Telescopes*, J. Mather, ed., *Proc. SPIE* **5487**, pp. 186–2000, 2004.

Abstract

PUBLICATIONS

Analysis of K-band imaging of the wide binary system σ CrB with the Lick Observatory NGS AO system

Kenneth J. Mighell, Julian C. Christou, Jack D. Drummond

Publication: Proc. SPIE Vol. 6272, 62720I, Advances in Adaptive Optics II; Brent L. Ellerbroek, Domenico Bonaccini Calia; Eds.

Publication Date: Jul 2006

Abstract

We present astronomical results from K-band adaptive optics (AO) observations of the wide binary system σ Corona Borealis with the Lick Observatory natural guide star adaptive optics system on 2004 August 27-29. Seeing conditions were excellent and the AO compensation was very good, with Strehl ratios reaching 50% at times. The stellar images were reduced using three different analysis techniques: (1) Parametric Blind Deconvolution, (2) Multi-Frame Blind Deconvolution, and (3) the MATPHOT stellar photometry code. The relative photometric and astrometric precision achievable with these three analysis methods are compared. Future directions that this research can go towards achieving the goal of routinely obtaining precise and accurate photometry and astrometry based on near-infrared AO observations are described.

« Return to Search Results

"Analysis of K-band imaging of the wide binary system σ CrB with the Lick Observatory NGS AO system", Mighell, K. J., Christou, J. C., & Drummond, J. D., in *Advances in Adaptive Optics II*, edited by B. L. Ellerbroek and D. B. Calia, Proc. SPIE Vol. 6272, pp. 62720I-1 to 62720I-6

Analysis of K-band Imaging of the Wide Binary System σ CrB with the Lick Observatory NGS AO System

Kenneth J. Mighell[a], Julian C. Christou[b], Jack D. Drummond[c]

[a]National Optical Astronomy Observatory, 950 N. Cherry Ave., Tucson, AZ 85719, U.S.A.;
[b]Center for Adaptive Optics, University of California, 1156 High St., Santa Cruz, CA 95064, U.S.A.;
[c]Starfire Optical Range, Directed Energy Directorate, Air Force Research Laboratory, Kirtland AFB, NM 87117, U.S.A.

ABSTRACT

We present astronomical results from K-band adaptive optics (AO) observations of the wide binary system σ Corona Borealis with the Lick Observatory natural guide star adaptive optics system on 2004 August 27–29. Seeing conditions were excellent and the AO compensation was very good, with Strehl ratios reaching 50% at times. The stellar images were reduced using three different analysis techniques: (1) Parametric Blind Deconvolution, (2) Multi-Frame Blind Deconvolution, and (3) the MATPHOT stellar photometry code. The relative photometric and astrometric precision achievable with these three analysis methods are compared. Future directions that this research can go towards achieving the goal of routinely obtaining precise and accurate photometry and astrometry based on near-infrared AO observations are described.

Keywords: binaries, astrometry, photometry, adaptive optics techniques, infrared instrumentation

1. INTRODUCTION

Adaptive optics (AO) photometry and astrometry of binary stars is problematic.[1] Photometry from AO observations of binary stars can exhibit errors (variations) which are larger than expected from simple noise analysis.[2,3] Anisoplanatism and scintillation[1] are contributing factors to this observed variation, but other sources of photometric error include calibration errors, such as residual flat-fielding errors, and instrumental/detector errors, such as the location of the sources on the detector[4] or *intrapixel* quantum efficiency variation in state-of-the-art optical and near-infrared cameras.[5,6]

Photometric reduction errors can also be significant source of variation in AO observations of binaries. The proper measurement of the background sky level is essential yet is frequently surprisingly difficult in many AO observations of multiple star systems. Ground-based non-AO imagers generally have Point Spread Functions (PSFs) which are characterized as having most of their power at low spatial frequencies due to the combination of atmospheric turbulence and dome seeing. Space-based PSFs frequently have significant amounts of power at higher spatial frequencies due to the lack of blurring caused by atmospheric turbulence. AO imagers generally produce PSFs with characteristics found in both uncorrected ground-based PSFs and space-based PSFs: low-spatial-frequency features (e.g., broad halos) are combined with high-spatial-frequency features (e.g., sharp central cores and rings of the Airy pattern). Although the human eye is drawn to the sharp core of the AO PSF, that core frequently contains only a small fraction of the total energy from a given star; very large photometric apertures are typically required in order to achieve even 90% of the encircled energy. If the determination of the background "sky" level is based on the analysis of values of pixels that are too close to the core of the AO PSF, then the total flux of the star can be significantly underestimated in a way that can lead to *systematic* rather than random photometric errors. The fact that atmospheric turbulence typically causes the PSF to vary from short exposure to short exposure just makes the precision analysis of AO binary star observations that much more challenging.

In this article, we present astronomical results from K-band AO observations of the wide binary system σ Corona Borealis (σ CrB) with the Lick Observatory natural guide star adaptive optics system. This astrometric calibrator was chosen because the large separation between the two components would help minimize the many measurement challenges facing AO observations of binary systems that were mentioned above. Section 2 describes these observations and their reductions using three different analysis techniques: (1) Parametric Blind Deconvolution, (2) Multi-Frame Blind Deconvolution, and (3) the MATPHOT stellar photometry code. The relative photometric and astrometric precision achievable with these three analysis methods are discussed and compared in Section 3. The article concludes in Section 4 with a discussion of the future directions that this research can go towards achieving the goal of routinely obtaining precise and accurate photometry and astrometry based on near-infrared AO observations.

2. OBSERVATIONS AND REDUCTIONS

Observations of the wide binary system σ CrB (a.k.a. WDS J16147+3352, ADS 9979 AB, STF 2032) were obtained at the Lick Observatory 3-m Shane Telescope using the natural guide star (NGS) adaptive optics system[7] with the IRCAL infrared imager[8] on the nights of 2004 August 27-29. These observations were obtained in the K-band with a Brackett-γ filter we label $K(Br\gamma)$ ($\lambda_0 = 2.167$ μm; $\delta\lambda = 0.020$ μm). The seeing conditions were very good during the observing run with coherence length, r_0 (550 nm) values ranging from 8-18cm. The AO performance is typically characterized by the Strehl ratio with perfect performance, i.e. no aberrations in the optical system, having a value of 100%. The measured K-band Strehl ratios for a number of point source stars throughout the run ranged from 30-60%; a detailed discussion of the Strehl ratio calculation is given in Section 4 of Ref. 4.

The nominal image scale for the IRCAL camera is $0.076''$ pixel^{-1} so that the K-band observations are critically sampled with a theoretical resolution (λ/D) of $0.149''$. Figure 1 shows a single frame K-band observation of σ CrB. The diffraction-limited cores are clearly visible as well as the residual halo structure, due to the uncompensated components of the wavefront. The effects of the spiders are also seen in the Point Spread Functions (PSFs). Fig. 1 shows the strong degree of similarity in the structure between the widely separated PSFs.

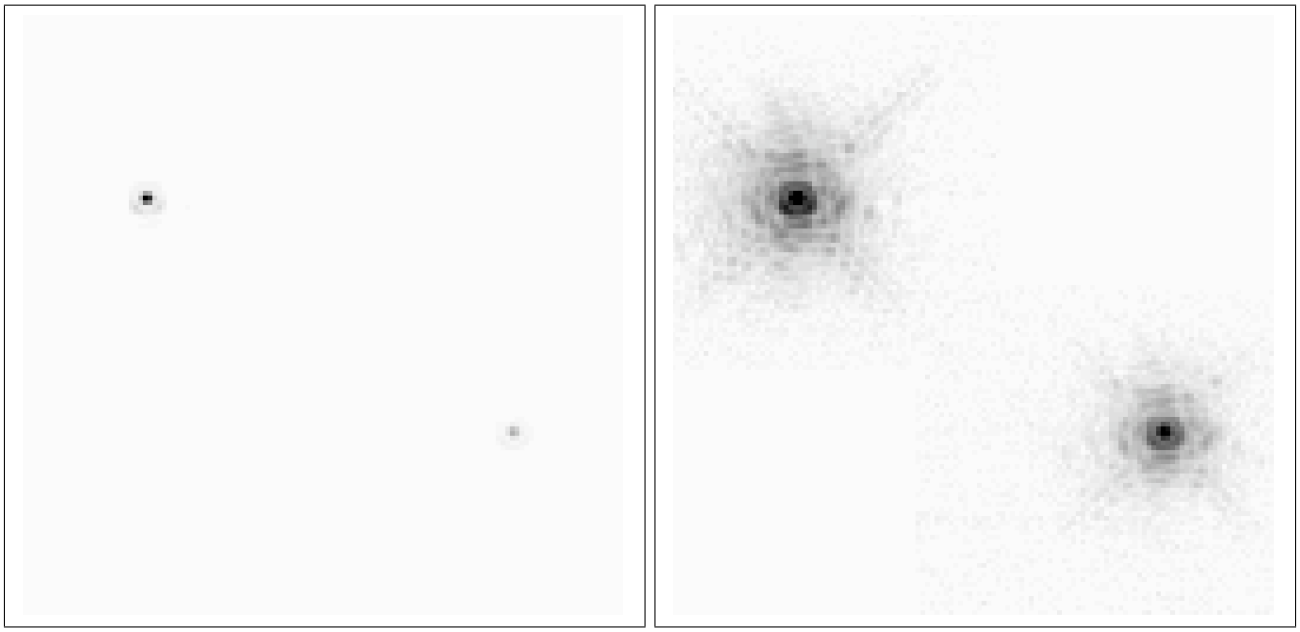

Figure 1. A portion of a single K-band observation of σ CrB obtained with the IRCAL infrared imager. The left side shows a linear stretch which emphasizes the bright central cores of the primary and secondary stars in this wide binary system. The right side shows a logarithmic stretch which emphasizes the faint halos as well as the effects of the spiders.

Each set of observations consisted of a series of short exposures (0.057-10 sec) which were initially preprocessed by sky-subtraction. The astrometry and photometry of the stars were obtained by three independent methods, Parametric Blind Deconvolution, Multi-frame Blind Deconvolution, and the MATPHOT[6] stellar photometry code. The first two techniques have been previously successfully applied to binary star, multiple star and cluster adaptive optics observations;[3,4,9] this is the first time the last technique has been applied to AO observations of binary stars.

Parametric Blind Deconvolution (PBD) models each of the PSFs in the image as a two-dimensional elliptical Lorentzian profile, which has been found to be an appropriate model for AO images. For this application, a Lorentzian profile was fit to each component in each of the separate frames in order to take into account any PSF variability across the field, i.e. anisoplanatism. A weighted mean, with the weights coming from the uncertainties of the fits, was computed for the separation angle (Sep), position angle (PA) and magnitude difference (Δm) for both stellar components. The PSFs in Figure 1 show departures from a Lorentzian model in that Airy rings are clearly visible. We compared the relative photometry and astrometry obtained from a Lorentzian fit to those obtained from a combined Lorentzian and Airy function fit to an observation of the multiple star system ι Cas (taken during this observation run) and found that the results did not change (within the dispersion of the measurements) which justified the use of the the simpler parametric model for the analysis of the σ CrB observations.

Multi-frame Blind Deconvolution (MFBD) finds a common solution to a set of independent images of the same field assuming that the PSF varies from one frame to the next. The series of observations were broken into smaller subsets, typically four per set of observations, and a deconvolved image was computed with each component constrained to have a Gaussian shape at the end. The relative astrometry and photometry were computed by two-dimensional elliptical Gaussian fits to these deconvolved images. As for PBD, the weighted mean of the separation, position angle and magnitude difference were computed.

The MATPHOT[6] stellar photometry code uses discrete (sampled) Point Spread Functions consisting of a numerical table represented by a matrix in the form of a FITS[10] image. Discrete PSFs are shifted within an observational model using a 21-pixel-wide damped sinc function,

$$f^{\text{shifted}}(x_0) \equiv \sum_{i=-10}^{10} f(x_i) \frac{\sin\left(\pi(x_i - x_0)\right)}{\pi(x_i - x_0)} \exp\left(-\left[\frac{x_i - x_0}{3.25}\right]^2\right) , \tag{1}$$

and position partial derivatives are computed using a five-point numerical differentiation formula,

$$f\,'(x_i) \approx \frac{1}{12}\left[f(x_{i-2}) - 8\,f(x_{i-1}) + 8\,f(x_{i+1}) - f(x_{i+2})\right] . \tag{2}$$

Precise and accurate stellar photometry and astrometry are achieved with undersampled observations by using supersampled discrete PSFs that are sampled 2, 3, or more times more finely than the observational data. Although these numerical techniques are not mathematically perfect, they are sufficiently accurate for precision stellar photometry and astrometry due to photon noise which is present in all astronomical imaging observations.[6] The current C-language implementation[11] of the MATPHOT algorithm is based on a robust implementation[12,13] of the Levenberg[14]-Marquardt[15] method of nonlinear least-squares minimization. Detailed analysis of simulated space-based CCD stellar observations demonstrate that millipixel relative astrometry and millimag photometric precision is achievable with complicated discrete PSFs.[6]

The MATPHOT stellar photometry code was developed for the analysis of space-based CCD cameras with complicated PSFs. We report the results obtained from the extension of the MATPHOT algorithm to ground-based AO PSFs.

The position and intensity of the primary and secondary stars were measured using the MATPHOT demonstrator program, MPD,[6,11] with a discrete PSF derived from a normalized background-subtracted image of the primary star. As for PBD and MFBD, the weighted mean of the separation, position angle and magnitude difference were computed.

3. COMPARISON OF INDEPENDENT ANALYSIS TECHNIQUES

Christou and Drummond report[4] that on 2004 August 28.90 the binary system σ CrB had the following parameters: a position angle of $237\overset{\circ}{.}5 \pm 0.1$, a large separation angle of 7.032 ± 0.008 arcsec, and $K(Br\gamma)$ magnitude difference of 1.01 ± 0.01 mag between the primary and secondary stars; these values were the unweighted mean and standard deviation of the PBD and MFBD results. The unweighted mean minimizes the effect of any systematic errors in one or the other of the two independent methods by favoring neither of them.

The left and central panels of Fig. 2 show, respectively, images of the primary and secondary stars taken from a single 3-second observation. The right panel of Fig. 2 shows the residuals in the region of the secondary star after the MATPHOT analysis has removed its best observational model (fit) from the image of the secondary star. The images in Fig. 2 are displayed with histogram equalization stretches in order to maximize the information content of each image. This enables us to see the strong degree of similarity in the fine structure details of the halos of the primary and secondary stars. Note the excellent removal by MATPHOT of the residual halo structure which is due to the uncompensated components of the wavefront. The right panel of Fig. 2 is graphical evidence that this observation occurred in the regime of partial-anisoplanatism where variation occurs mainly in the stellar cores.

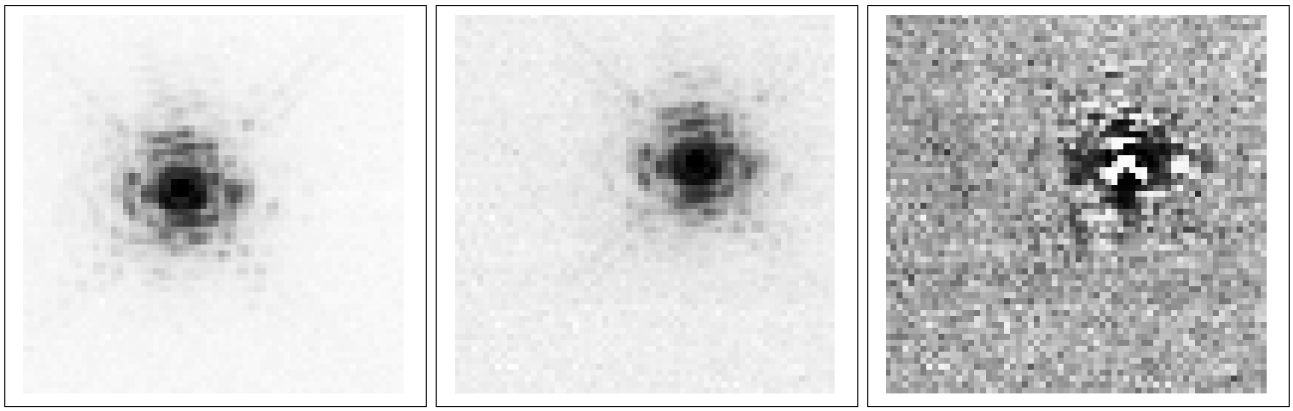

Figure 2. The primary *(left)* of σ CrB, the secondary *(middle)*, and the residuals left after fitting PSF to the secondary. Histogram equalization stretches were used for all images; the relative dynamic ranges are, from left to right, $26.9 : 10.3 : 1$.

The results from the independent MATPHOT analysis are statistically identical to those reported for the previous PBD and MFBD analysis: PA$= 237\overset{\circ}{.}5 \pm 0.1$, Sep$= 7.015 \pm 0.003$ arcsec, and $\Delta m = 1.02 \pm 0.01$ mag. The fact that three very different analysis techniques all yield the same answers, within the statistical uncertainties, enhances our confidence in these results.

Our rms errors of the measured separation angle between the primary and secondary stars of σ CrB in individual observations (typically 2–3 mas) is very small when compared to the nominal IRCAL pixel size of 76 mas or the diffraction spot size (λ/D) of 149 mas. This precision in the measurement of the separation angle of a wide binary system has revealed a residual non-linearity in the spatial calibration (i.e., pincushion aberration) of the IRCAL infrared imager which, although it is smaller than the diffraction spot size, is still quite significant because it can cause systematic astrometric errors if its existence is not recognized.[4]

4. FUTURE DIRECTIONS

While the results of this study are quite encouraging for the future prospects for precision stellar photometry and astrometry using near-infrared detectors on adaptive optics systems, much work remains to be done before 1% photometry and milliarcsec relative astrometry are routinely achieved. Working with these observations has given us some insight on possible ways to improve ground-based near-infrared adaptive optics.

Ground-based observers using state-of-the-art infrared AO cameras at premier observing sites are now able to achieve milliarcsec spatial resolutions with near-diffraction-limited optics. For example, our natural guide star

AO observations with the IRCAL infrared imager yielded astrometric measurements with an angular resolution of just 2% of the diffraction spot size of a 3-m telescope (149 mas) and less than 5% the size of a small (76 mas) AO camera pixel. The fact that three independent AO stellar image analysis techniques are precise enough to reveal the existence of calibration errors in a state-of-the-art AO camera reveals the need for better (more accurate) plate scale calibrations for the detectors placed behind AO systems — if the full potential for relative astrometry with near-infrared AO stellar observations is to be reached. Better calibrations will require better astrometric calibrators, the creation of which will require the allocation of many observing nights with excellent seeing conditions on medium-to-large telescopes.

Searching for commonalities in different PSFs obtained with the same AO camera system on nights of similar excellent seeing conditions may now be feasible using image analysis tools like the MATPHOT stellar photometry code. Such a calibration effort may reveal an underlying non-negligible telescope-camera footprint on the PSF which is either stable on a nightly basis or varies slowly in a predictable manner possibly as a function of temperature. That knowledge could be combined with modeling of the atmospheric turbulence above the telescope and of the AO system itself to improve our ability to produce real-time predictions of the AO system PSF from real-time engineering information about the telescope and AO system — possibly including state information of individual actuators in the deformable mirror(s) within the optical path.

Having investigated the current limits of relative AO photometry and astrometry with a wide binary system, the next step is to see if the same precision levels can be achieved in studies of close binaries with overlapping PSFs and ultimately in very crowded stellar fields like that found near the Galactic center. While this investigation used a "simple" PSF, the MATPHOT algorithm was designed to handle complicated PSFs from space-based segmented telescopes (e.g., the *James Webb Space Telescope*); it would be very interesting to determine if these techniques will work as well with complicated PSFs from state-of-the-art laser guide star AO observations like those produced by the LGSAO system of the Keck II 10-m telescope (see Fig. 1 of Ref. 16).

Finally, the process of doing MATPHOT analysis on these observations has provided insights towards ways to improve the MATPHOT stellar photometry code so that it is more flexible, robust and easier to use. For example, the shift from optical to the near infrared has revealed the need to give the MATPHOT code the ability to use "error maps" associated with the observational data. Optical CCD stellar observations typically can be characterized with a simple noise model based on photon statistics (Poisson distributions) and shot noise (Gaussian distributions), while near-infrared stellar AO observations usually have their backgrounds subtracted – which can makes it very difficult, if not impossible, to create a reliable noise model for a near-infrared observation based on assumptions which were valid for optical CCD observations. Giving MATPHOT the ability to use "error maps" — generally produced by calibration pipelines — not only relieves the program from the burden of having to produce a noise model of the observation, but it also makes the program more flexible in its ability to work with optical and infrared observations.

ACKNOWLEDGMENTS

We would like to thank the staff of Lick Observatory, in particular Elinor Gates, the AO Support Scientist for her valuable assistance with the AO system, and also many useful discussion with Donald Gavel. This work has been supported by a grant from the National Aeronautics and Space Administration (NASA), Interagency Order No. NNG05EB61I, which was awarded by the Applied Information Systems Research (AISR) Program of NASA's Science Mission Directorate and by the National Science Foundation Science and Technology Center for Adaptive Optics, managed by the University of California at Santa Cruz under cooperative agreement No. AST - 9876783.

REFERENCES

1. L. C. Roberts, et al., "Adaptive optics photometry and astrometry of binary stars," *AJ* **130**, pp. 2262–2271, 2005.
2. T. A. ten Brummelaar, et al., "Scientific results using the Mount Wilson Institute adaptive optics system," in *Adaptive Optical System Technologies*, D. Bonaccini and R. K. Tyson, eds., *Proc. SPIE* **3353**, pp. 391–397, 1998.

3. D. Barnaby, E. Spillar, J. C. Christou, and J. D. Drummond, "Measurements of binary stars with the Starfire Optical Range adaptive optics systems," *AJ* **119**, pp. 378–389, 2000.
4. J. C. Christou and J. D. Drummond, "Measurements of binary stars, including two new discoveries, with the Lick Observatory adaptive optics system," *AJ* **(in press)**, 2006.
5. T. R. Lauer, "The photometry of undersampled point-spread functions," *PASP* **111**, pp. 1434–1443, 1999.
6. K. J. Mighell, "Stellar photometry and astrometry with discrete point spread functions," *MNRAS* **362**, pp. 861–878, 2005.
7. B. J. Bauman, et al., "New optical design of adaptive optics system at Lick Observatory," in *Adaptive Optics Systems and Technology*, R. K. Tyson and R. Q. Fugate, eds., *Proc. SPIE* **3762**, pp. 194–200, 1999.
8. J. P. Lloyd, et al., "IRCAL: the infrared camera for adaptive optics at Lick Observatory," in *Optical and IR Telescope Instrumentation and Detectors*, M. Iye and A. F. Moorwood, eds., *Proc. SPIE* **4008**, pp. 814–821, 2000.
9. J. D. Drummond, "Adaptive optics Lorentzian point spread function," in *Adaptive Optical System Technologies*, D. Bonaccini and R. K. Tyson, eds., *Proc. SPIE* **3353**, pp. 1030–1037, 1998.
10. FITS Support Office web site: `http://fits.gsfc.nasa.gov` .
11. MATPHOT web site: `http://www.noao.edu/staff/mighell/matphot` .
12. K. J. Mighell, "Accurate stellar photometry in crowded fields," *MNRAS* **238**, pp. 807–833, 1989.
13. K. J. Mighell, "Algorithms for CCD stellar photometry," in *Astronomical Data Analysis Software and Systems VIII*, D. M. Mehringer, R. L. Plante, and D. A. Roberts, eds., *ASP Conference Series* **172**, pp. 317–328, 1999.
14. K. Levenberg, "A method for the solution of certain problems in least squares," *Quarterly of Applied Mathematics* **2**, pp. 164–168, 1944.
15. D. Marquardt, "An algorithm for least-squares estimation of nonlinear parameters," *SIAM Journal of Applied Mathematics* **11**, pp. 431–441, 1963.
16. A. M. Ghez, et al., "The First Laser Guide Star Adaptive Optics Observations of the Galactic Center: Sgr A*'s Infrared Color and the Extended Red Emission in its Vicinity," *ApJ* **635**, pp. 1087–1094, 2005.

Title:	Mitigating the Impact of Large Intrapixel Quantum Efficiency Variations on Precision Stellar Photometry and Astrometry
Authors:	Mighell, K. J.
Affiliation:	AA(NOAO)
Publication:	American Astronomical Society Meeting 207, #23.03; Bulletin of the American Astronomical Society, Vol. 37, p.1196
Publication Date:	12/2005
Origin:	AAS
Abstract Copyright:	(c) 2005: American Astronomical Society
Bibliographic Code:	2005AAS...207.2303M

Abstract

Current infrared detector technology can produce imagers with non-uniform intrapixel response functions. This can cause significant stellar flux loss (depending on where a star is centered within the central pixel) which is an observational fact in some existing space-based astronomical cameras. Large intrapixel quantum efficiency (QE) variations can also cause the observed (apparent) positions of stars to be significantly corrupted. With such ugly detectors, the observed stellar brightnesses and positions are neither precise or accurate. Excellent stellar photometry and astrometry is, fortunately, still achievable even in the presence of large intrapixel QE variations --- as long as the image formation process inside the detector is accurately modeled within the photometric reduction code. Detailed analysis of simulated space-based stellar observations are presented which demonstrate how the impact of large intrapixel QE variations can be mitigated using the MATPHOT algorithm with accurate discrete Point Spread functions and accurate Detector Response Functions. Source code and documentation for MATPHOT and support software is freely available at the following web site: http://www.noao.edu/staff/mighell/matphot K.J.M was supported by a grant from the National Aeronautics and Space Administration (NASA), Interagency Order No. NNG05EB61I, which was awarded by the Applied Information Systems Research (AISR) Program of NASA's Science Mission Directorate.

Use: ☐ Authors
☑ Title
☑ Abstract Text
Return: ◉ Query Results Return 100 items starting with number 1
○ Query Form
Database: ☑ Astronomy
☐ Physics
☐ arXiv e-prints
Send Query Reset

Smithsonian/NASA ADS Homepage | ADS Sitemap | Query Form | Basic Search | Preferences | HELP | FAQ

Mitigating the Impact of Large Intrapixel Quantum Efficiency Variations on Precision Stellar Photometry and Astrometry

Kenneth Mighell
National Optical Astronomy Observatory
mighell@noao.edu

ABSTRACT

Current infrared detector technology can produce imagers with non-uniform intrapixel response functions. This can cause significant stellar flux loss (depending on where a star is centered within the central pixel) which is an observational fact in some existing space-based astronomical cameras. Large intrapixel quantum efficiency (QE) variations can also cause the observed (apparent) positions of stars to be significantly corrupted. With such ugly detectors, the observed stellar brightnesses and positions are neither precise or accurate. Excellent stellar photometry and astrometry is, fortunately, still achievable even in the presence of large intrapixel QE variations --- as long as the image formation process inside the detector is accurately modeled within the photometric reduction code. Detailed analysis of simulated space-based stellar observations are presented which demonstrate how the impact of large intrapixel QE variations can be mitigated using the MATPHOT algorithm with accurate discrete Point Spread functions and accurate Detector Response Functions (Mighell 2005, MNRAS, 361, 861). Source code and documentation for MATPHOT and support software is freely available at the following website: http://www.noao.edu/staff/mighell/matphot

What you see is *not* what you can get!

Fig. 1 shows a simulated *Next Generation Space Telescope (NGST) V*-band CCD stellar observation.

Fig. 2 Many state-of-the art near-infrared detectors have large intrapixel quantum efficiency variations. Suppose we have a detector where only 56.25% of each pixel is 100% active and the rest has zero QE response. This figure shows what happens when such a detector is used to simulate *NGST* observations – the amount of electron loss varies significantly across each detector (pixel).

Fig. 3 shows that stellar magnitudes reported by the MATPHOT algorithm are precise and accurate while the observed magnitudes are neither.

Fig. 4 shows that stellar positions reported by MATPHOT are precise and accurate while the observed stellar positions have large systematic errors.

Fig. 5 shows that the MATPHOT algorithm can produce precise and accurate stellar photometry for bright and faint stars with ugly discrete Point Spread Functions and ugly detectors featuring large intrapixel quantum efficiency variations.

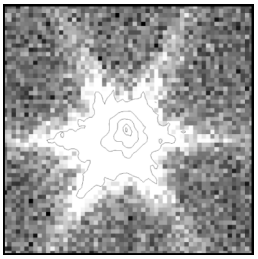

Figure 1. A simulated *V*-band *Next Generation Space Telescope* CCD image based on a 2 x 2 supersampled PSF model for a 8-meter TRW-concept 1.5-micron diffraction-limited primary mirror with 1/13 rms wave errors. Contour levels of 90%, 50%, 10%, 1%, and 0.1% of the peak intensity are shown with *black curves*. The pixel scale is 0.0128 arcsec px^{-1}; the original version of the PSF was kindly provided by John Krist (JPL).

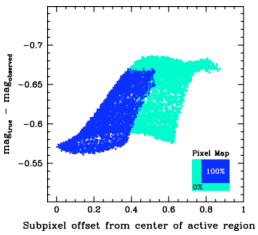

Figure 2. The measured electron loss of 10,000 simulated CCD observations of -15 mag (10^6 photons) stars analyzed with **mpdx** using a 4 x 4 supersampled version of the *NGST* PSF described in Fig. 1.

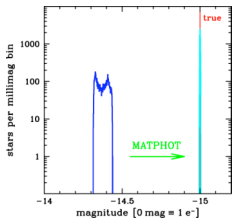

Figure 3. The observed *(left)* and the measured *(right)* stellar magnitude of the 10,000 -15 mag stars described in Fig. 2. **Note that the *observed stellar magnitudes were neither precise nor accurate*.**

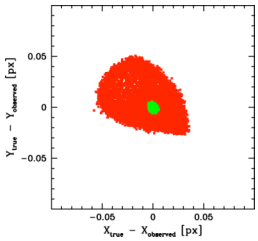

Figure 4. The difference between the true and observed (red) and measured (green) positions of the 10,000 -15 mag stars described in Fig. 2. **Note the *large systematic errors in the observed positions*.**

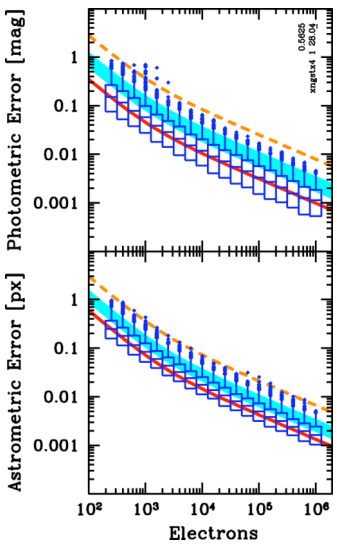

Figure 5. The absolute photometric errors *(top)* and total astrometric errors *(bottom)* of 20,000 simulated *NGST* CCD stellar observations analyzed with **mpdx** using a 4 x 4 supersampled version of the *NGST* PSF ($\beta \approx 28.04$ px^2; V = 0.5625).

ACKNOWLEDGEMENT

This work is supported by a grant from the National Aeronautics and Space Administration (NASA), Interagency Order No. NNG05EB61I (NRA 03-OSS-01), which was awarded by the Applied Information Systems Research (AISR) program of NASA's Science Mission Directorate.